Food Hydrocolloids 156 (2024) 110313

Contents lists available at ScienceDirect

Food Hydrocolloids

journal homepage: www.elsevier.com/locate/foodhyd

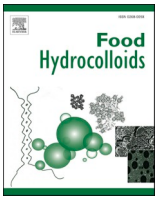

Molecular, interfacial and foaming properties of pulse proteins

Penghui Shen [a], Jinfeng Peng [b], Leonard M.C. Sagis [a], Jasper Landman [a,*]

[a] Laboratory of Physics and Physical Chemistry of Foods, Wageningen University, Bornse Weilanden 9, 6708, WG, Wageningen, the Netherlands
[b] Danone Global Research & Innovation Center, Utrecht, the Netherlands

ARTICLE INFO

Keywords:
Pulse proteins
Air-water interface
Interfacial adsorption kinetics
Interfacial dilatational rheology
Interfacial structure
Foam

ABSTRACT

Pulses are important protein sources in the current protein transition, but much of the behavior of pulse proteins in food systems (e.g. foam) is still unknown. This study compared the similarities and differences of the proteins from three common pulses: lentil, faba bean, and chickpea, at the molecular, mesoscopic and functionality levels. For each source, the proteins were extracted with a simple one-pot alkaline extraction, resulting in protein extracts with high protein content (67–85%) rich in globulins (68–81%) and albumins (19–32%). All pulse protein fractions were predominantly in a native state with high solubilities (83–91%), high denaturation enthalpies (8.9–10.1 J/(g protein)) and low aggregation levels. Lentil protein showed higher absolute value of the ζ-potential (−18.5 ± 1.2 mV) than faba bean (−13.2 ± 0.8 mV) and chickpea protein (−12.4 ± 1.2 mV). The behavior of all pulse proteins at the air-water interface including adsorption kinetics, interfacial dilatational rheology and interfacial microstructure was investigated and linked to their foaming properties. The pulse protein with the highest vicilin and convicilin content (39.5% in lentil protein) showed the shortest adsorption lag time (300 ms), and demonstrated the highest foam overrun (290 ± 17%). All three pulse protein fractions formed interfaces with disordered solid-like behavior and consisted of heterogeneous network structures. These structures were mostly comprised of intact globulin proteins for lentil and faba bean proteins, while mixtures of intact globulins and unfolded proteins/albumins were observed for chickpea protein. The interfacial stiffness, interfacial density and ζ-potential of these pulse proteins showed a high positive correlation with their foam stabilization properties. Lentil protein has the highest values of those parameters and showed the longest foam half-life time of 115 (± 22) min, while faba bean and chickpea proteins showed comparably lower values of those parameters and shared similarly shorter foam half-life times of 46 (± 19) min and 38 (± 6) min, respectively. These findings can aid to provide clearer directions in screening pulse proteins for desirable performance in aerated food products.

1. Introduction

Pulses have been cultivated for thousands of years and nowadays are consumed throughout the world (Kumar & Pandey, 2020). They are highly versatile, and there are 700–800 genera and around 19,000 systematized species of pulse crops. Of these genera, twelve are economically the most important (Raikos, Neacsu, Russell, & Duthie, 2014). Pulses are highly productive with a total worldwide production of more than 92 million tons in 2018 (Kumar et al., 2020). They are rich in protein with protein content of 19–40 wt% (on dry basis) (Boukid, Zannini, Carini, & Vittadini, 2019; Raikos et al., 2014). Therefore they are important protein sources for human consumption (Didinger & Thompson, 2022; Shevkani, Singh, Chen, Kaur, & Yu, 2019). Compared to the production of animal-based products, the production of pulses has a much lower environmental impact (Detzel et al., 2022; Vogelsang-O'Dwyer et al., 2020), and can reduce greenhouse gas emission, conserve water, and protect water and soil (Adarsh, Jacob, & Giffy, 2019; Khiangte & Siddique, 2021; Snyder, Bruulsema, Jensen, & Fixen, 2009). Therefore, pulses are among the most important sources to supply food proteins for addressing sustainability and food security concerns (Aiking & de Boer, 2020; Bessada, Barreira, & Oliveira, 2019).

Lentil, faba bean and chickpea are among the most cultivated and/or consumed pulses, and are popular among consumers (Boukid, 2021; Ehsani, Westphalen, Doan, Lohi, & Abdelrasoul, 2024; Henn, Zhang, Thomsen, Rinnan, & Bredie, 2022; Vogelsang-O'Dwyer, Zannini, & Arendt, 2021). The proteins from these pulses have good nutritional properties and various biological activities (Boukid, 2021; Gandhi, Toor, Kaur, & Kaur, 2022; S. Sharan et al., 2021), and also possess good

* Corresponding author.
E-mail address: Jasper.Landman@wur.nl (J. Landman).

https://doi.org/10.1016/j.foodhyd.2024.110313
Received 4 April 2024; Received in revised form 3 June 2024; Accepted 12 June 2024
Available online 12 June 2024

techno-functionalities, such as high solubility (80–90% at neutral pH) (Yaputri, Bu, & Ismail, 2023; Jarpa-Parra, 2018; Shi & Nickerson, 2022) and high foaming properties (Jarpa-Parra, 2018; Shi et al., 2022; Tang, Roos, & Miao, 2023). Due to these benefits, they have great potential as substitutes for animal-based proteins (Alu'datt et al., 2017; Buhl, Christensen, & Hammershøj, 2019; Vogelsang-O'Dwyer et al., 2021). They have been applied to replace dairy and egg proteins in foam-based food products such as cakes and muffins, with satisfying sensory properties (Jarpa-Parra et al., 2017; Zhao et al., 2022).

Foam is one of the most important food systems. In food, proteins are typically used to stabilize the air-water interface in foam (Amagliani, Silva, Saffon, & Dombrowski, 2021; Nasrollahzadeh, Nezafat, & Shafiei, 2021; Wierenga & Gruppen, 2010). Many studies have investigated the foaming properties of lentil, faba bean and chickpea proteins primarily at the macroscopic level (Amagliani et al., 2021; Grasso, Lynch, Arendt, & O'Mahony, 2022; Jarpa-Parra, 2018; S. Sharan et al., 2021), but the interfacial stabilization mechanisms are much less explored. The behavior of lentil protein at the air-water interface and in foam stabilization was systematically investigated in our recent study (Shen, Peng, Sagis, & Landman, 2024); faba bean and chickpea proteins are less well studied and their behavior is still largely unknown. Globulins (including legumin globulins and vicilin globulins) and albumins constitute the main part of water-soluble proteins in lentils, faba beans and chickpeas (Boye, Zare, & Pletch, 2010; Kiosseoglou, Paraskevopoulou, & Poojary, 2021; Martineau-Cote, Achouri, Karboune, & L'Hocine, 2022). These three sources have different globulin-to-albumin ratios and different legumin-to-vicilin ratios (Vogelsang-O'Dwyer, Sahin, Arendt, & Zannini, 2022). Albumins and globulins have totally different physicochemical properties (e.g. surface charge, surface hydrophobicity and molecular weight) and have shown pronouncedly different behaviors at air-water interfaces (Shen, Yang, Nikiforidis, Mocking-Bode, & Sagis, 2023; Yang, de Wit, et al., 2022). For example, rapeseed albumin has been shown to have a much faster adsorption rate to air-water interfaces compared to rapeseed globulin, due to its much smaller size (1.5 nm) compared to rapeseed globulin (10 nm), and displayed significantly higher foam overrun (410%) than rapeseed globulin (320%) (Shen et al., 2023). The albumins of mung bean, Bambara groundnut and pea formed much stiffer interfaces than their respective globulin fractions, and displayed considerably higher foam stability, while within the globulin fractions themselves, legumins and vicilins also demonstrated different behaviors at interface and in foam (Yang, de Wit, et al., 2022). Legumins are physicochemically rather different from vicilins. For example, legumins are hexamers with molecular weights of 300–400 kDa, and disulfide bonds are involved in subunit stabilization, while vicilins are trimers with molecular weights of 145–190 kDa, and lack disulfide bonds in their molecular structures (Shevkani et al., 2019). Thus, lentil, faba bean and chickpea proteins are expected to have different behaviors at air-water interfaces and in foam stabilization.

In our recent study, we showed that mildly extracted lentil protein had comparable foamability to both whey protein and egg white protein, and similar foam stability to egg white protein (Shen et al., 2024). We elucidated the air-water interface and foam stabilization mechanism of the mildly extracted lentil protein: the fast adsorption of lentil protein at the air-water interface gave it high foam overrun, and the mostly intact globulin particles at the air-water interface resulted in high interfacial thickness and a stiff and stretchable interfacial structure, giving the foam a long half-life time (Shen et al., 2024). In this study, we further investigated the air-water interface and foam stabilization behavior of faba bean and chickpea proteins in comparison to lentil protein, with the same methodology. Firstly, we extracted faba bean and chickpea proteins in the same way as for lentil protein extraction, and systematically studied their physicochemical properties (e.g. particle size, surface charge, protein composition and nativity). We also studied their adsorption behavior at the air-water interface on both short-time (sub-second) and long-time scales, followed by the study of the mechanical properties of generated interfacial films using small amplitude and large amplitude oscillatory dilatational rheology. We also measured the interfacial thickness using ellipsometry and studied the interfacial morphology using Langmuir-Blodgett deposition combined with atomic force microscopy (AFM). Finally, we compared the air-water interface and foam stabilization behavior of lentil, faba bean and chickpea proteins, and identify and discuss several important factors for pulse proteins important for their ability to stabilize foam. These findings can give theoretical support for a better understanding of the similarities and differences between pulse proteins in foam stabilization, and guide the utilization of pulse proteins in the design of aerated food products.

2. Materials and methods

2.1. Materials

Split red lentil, faba bean and chickpea were bought from local pulse suppliers. All chemicals (Sigma-Aldrich, USA) were used as received. Ultrapure water (MilliQ Purelab Ultra, Germany) was used for all experiments unless stated otherwise.

2.2. Methods

2.2.1. Protein extraction

All pulse proteins were extracted with the same alkaline extraction method. They were first milled into fine power with a Hosokawa Multimill (Hosokawa Alpine, Augsburg, Germany) equipped with a UPZ fine impact mill. The powder was then mixed with ultrapure water at a ratio of 1:10 (w/w) and adjusted to pH8 using 1 M NaOH solution under magnetically stirring for 1 h. After that, the suspension was centrifuged in different conditions: 17000 g, 20 min and 20 °C for the lentil powder suspension; 8000 g, 20 min and 20 °C for the faba bean powder suspension; 17000g, 1 h and 20 °C for the chickpea powder suspension. The centrifugation of the chickpea powder suspension took much longer because of the presence of a significant amount of oleosomes, which would form a top layer only after prolonged centrifugation. After centrifugation, the aqueous phase was collected and dialyzed over 3.5 kDa cut-off membranes against deionized water for 2 days. Water was replaced twice on each day. Finally, the retentate was freeze-dried, and the protein extract powder was stored at 4 °C.

2.2.2. Proximate analysis

The proximate analysis of the pulse protein extracts was performed according to our previous work (Shen et al., 2024). In brief, protein content was measured by using a Flash EA 1112 Series Dumas (Interscience, The Netherlands), and a conversion factor of 5.7 was used (Sosulski & Holt, 1980). Total starch content was measured by using an enzyme starch kit (Megazyme Inc., Ireland), following the manufacturer's instructions. Phenol content was measured by using a Folin-Ciocalteu assay, and the adsorption of mixtures at the wavelength of 725 nm was measured with gaulic acid as a standard. Oil content was measured by Soxhlet extraction using a Soxtherm Unit Sox416 (Gerhardt, Königswinter, Germany). Water content was measured by drying samples at 105 °C for 24 h. Ash content was measured by igniting samples at 550 °C for 24 h. All measurements were performed in triplicate.

2.2.3. Protein solubility

Samples were first dissolved in sodium phosphate buffer (pH7.0, 20 mM) at 1 wt% extract concentration overnight and then filtrated over 0.22 μm syringe filters. The protein content of the filtrates was determined by the dumas method as mentioned above and used to calculate the protein solubility. The measurement was performed in triplicate.

2.2.4. Protein dispersion preparation

All protein samples for later measurements were prepared at 0.1 wt% soluble protein concentration in sodium phosphate buffer (pH7.0, 20

mM) overnight, based on their protein solubilities, and were used after filtration through 0.22 μm syringe filters to remove all insoluble materials, unless stated otherwise.

2.2.5. Characteristics of protein extracts

2.2.5.1. Particle size and zeta potential. The particle size of pulse protein extracts was assessed by dynamic light scattering at a backscatter angle of 173° on a Zetasizer Nano ZS (Malvern Instruments, UK) at an extract concentration of 0.1 wt% in sodium phosphate buffer (pH7.0, 20 mM). The refractive index of protein was set as 1.450 (Guemouri, Ogier, & Ramsden, 1998), and that of water was set as 1.330. The zeta potential was determined by micro electrophoresis in the Zetasizer in the same conditions as the size measurement. All measurements were performed at 20 °C in triplicate.

2.2.5.2. Size exclusion chromatography (SEC). SEC was applied to determine the protein composition of pulse protein extracts on an Akta Pure 25 chromatography system (GE Healthcare, Diegem, Belgium) according to our previous study (Shen et al., 2024). In brief, a protein dispersion was prepared at 1 wt% extract concentration in sodium phosphate buffer (pH7.0, 20 mM, containing 150 mM NaCl) and hydrated overnight, followed by filtration through 0.45 μm syringe filters. Afterwards, 50 μL of sample was loaded on a Superdex 200 increase 10/300 GL column (Merck, Schnelldorf, Germany), and eluted with the same sodium phosphate buffer as used for dissolving protein extracts, at a flow rate of 0.75 mL/min. Protein was detected at a wavelength of 214 nm. A calibration curve was established by measuring a series of reference samples with known molecular weights, and these were blue dextran (2000 kDa), ferritin (440 kDa), aldolase (158 kDa), conalbumin (75 kDa), ovalbumin (44 kDa), carbonic anhydrase (29 kDa), ribonuclease A (13.7 kDa), and aprotin (6.5 kDa).

2.2.5.3. Nativity. The nativity of pulse protein extracts was evaluated using differential scanning calorimetry (DSC) on a Discovery DSC25 (TA Instruments, USA). Protein dispersions at 10 wt% extract concentration were prepared in sodium phosphate buffer (pH7.0, 20 mM) and hydrated overnight. Afterwards, 50 mg of the protein dispersion was added in a stainless-steel high-volume pan and sealed with a lid. The pan was then equilibrated at 20 °C for 5 min, followed by a temperature ramp to 140 °C at a rate of 5 °C/min. An empty pan was used as a reference, and nitrogen was used as carrier gas. The denaturation temperature and enthalpy were calculated by the TA Trios software. All measurements were performed at least in duplicate.

2.2.5.4. Surface hydrophobicity. The surface hydrophobicity of pulse protein extracts was measured using a fluorescence probe 8-anilino-1-napthalenesulfonic acid ammonium salt (ANSA) on an LS 50B luminescence spectrometer (PerkinElmer, USA). In sodium phosphate buffer (pH7.0, 20 mM), ANSA solution was prepared at a concentration of 8 mM, and protein dispersions were prepared at a soluble protein concentration of 0.1 wt% and diluted to 0–0.03 wt%. Afterwards, 3 mL of protein dispersion was mixed with 25 μL of ANSA solution, and the mixture was incubated at room temperature in the dark for 1 h. Subsequently, the fluorescence intensity of the mixture was measured at an excitation wavelength of 390 nm and an emission wavelength of 470 nm. The slope of the linear regression of the fluorescence intensity as a function of protein concentration was taken as a measure for the surface hydrophobicity of proteins. The measurements were performed at least in duplicate.

2.2.6. Interfacial adsorption

The interfacial adsorption behavior of the pulse proteins was measured using a bubble pressure tensiometer (BPT) (BPT mobile, Krüss GmbH, Hamburg, Germany) for the short-time scale of adsorption, according to our previous study (Shen et al., 2024), and on an automatic drop tensiometer (ADT) (Tracker, Teclis, Longessaigne, France) for the long-time scale of adsorption. On the BPT, air bubbles were consecutively generated from a capillary tip (SH2510) into a protein dispersion (0.1 wt%), of which 15 mL was filled into a glass cuvette. The pressure within the air bubbles was monitored by BPT and transferred to surface tension by the in-built software. On the ADT, an air bubble with area of 12 mm^2 was first formed at the tip of a curved needle that was immersed in a protein dispersion (0.1 wt%), and controlled via a 500 μL air-tight glass syringe (SGE, Supelco, Sigma-Aldrich). The bubble profile was captured by a CCD camera system and fitted with the Young-Laplace equation to calculate the surface tension by the in-built software, in which the density of air phase was set to 0.0012 g/cm^3, and that of aqueous phase was set to 0.998 g/cm^3. The surface tension was monitored for 3 h. All measurements were performed at room temperature (around 20 °C) and in at least triplicate. Surface pressure was calculated by subtracting the surface tension of the samples from the surface tension of the clean air-water interface.

2.2.7. Interfacial dilatational rheology

To monitor the evolution of the interfacial stiffness with time, small amplitude oscillatory dilatational rheology (SAOD) with an amplitude of 3%, and frequency of 0.02 Hz was performed during interfacial adsorption for 5 h. We also performed oscillatory dilatational frequency sweeps (0.0067–0.067 Hz, at a fixed amplitude of 3%) and amplitude sweeps (2–50% strain, at a fixed frequency of 0.02 Hz), after allowing the proteins to adsorb at the air-water interface for 3 h, without being disturbed. Five cycles were conducted for each condition, followed by a recovery time of 50 s, before the next oscillation was started. The interfacial elastic modulus ($E_d^{'}$) and viscous modulus ($E_d^{''}$) were calculated by Fourier transformation, using the in-built software. We also constructed Lissajous plots of surface pressure (the surface tension at time t minus the surface tension after 3 h of adsorption) versus intracycle strain ($=(A(t)-A_0)/A_0$); A_0 is the surface area in the undeformed state, and it is 12 mm^2 in this study). The obtained Lissajous plots were further decomposed by the general stress decomposition (GSD) method established by de Groot, Yang, and Sagis (2023). All measurements were performed in at least triplicate at 20 °C.

2.2.8. Interfacial imaging

To image the interfaces formed by pulse proteins, Langmuir-Blodgett (LB) films were prepared using a Langmuir trough (KSV NIMA/Biolin Scientific Oy, Finland) according to our previous study (Shen et al., 2024). Briefly, the Langmuir trough was first filled with sodium phosphate buffer (pH7.0, 20 mM) and a freshly cleaved mica sheet was vertically immersed in the fluid (Highest Grade V1 Mica, Ted Pella, USA), followed by the injection of 200 μL of protein dispersion (0.1 wt %) at the trough bottom. Protein was allowed to adsorb to the air-water interface for 3 h, and the surface pressure was monitored by a Wilhelmy plate. Afterwards, the interface was compressed with two barriers at a speed of 5 mm/min. After the targeted surface pressure (13 and 23 mN/m) was reached during the compression, the compression slowed down to keep the targeted surface pressure while the mica was lifted at a speed of 1 mm/min, during which the interfacial film was gently transferred to the mica surface. The LB films were dried in a desiccator for two days and then imaged with atomic force microscopy (AFM) imaging.

The imaging was performed on a NanoWizard® 4XP AFM (Nano-Science, Bruker Nano GmbH, Germany) with the same method as used in our previous study (Shen et al., 2024). In short, the film was scanned in a PeakForce Tapping® mode using a PEAKFORCE-HIRS-F-A cantilever (Bruker Nano GmbH, Germany), of which the normal tip radius is only 1 nm. For each film, at least four images were captured over 2×2 μm^2 and 350×350 nm^2 area, in a lateral resolution of 512 x 512 $pixels^2$. The images were further processed using an built-in JPK data processing software (Bruker Nano GmbH, Germany).

2.2.9. Image analysis

The AFM images were subjected to image analysis with *Image J* for protein domain size determination and *AngioTool 64* software (National cancer Institute, National Institute of Health, Maryland, USA) for protein network evaluation according to our previous study (Shen et al., 2024). Briefly, in *image J*, AFM images were first inverted and transferred to 8-bit grayscale images, and then analyzed with the pair correlation function (g(r)) macro, producing a curve of g(r) as a function of distance r from a reference point. Subsequently, the curve was smoothed, and the r where g(r) decreases to 1 or the first minimum was taken as the protein domain size. The maximum value of g(r) was used to indicate the heterogeneity of the distribution of interfacial structure. Using *AngioTool 64*, the image of the interfacial structure was converted into vessel structures by applying a recursive Gaussian filter and multiscale Hessian enhancement filter, and further processed by segmentation and skeleton analysis, producing a series of network parameters such as vessel area, junction density, average vessel length and lacunarity (Zudaire, Gambardella, Kurcz, & Vermeren, 2011). An example of the output of this processing is given in Fig. S4. The lacunarity indicates the heterogeneity of the distribution of voids within structures, and lower lacunarity implies lower heterogeneity of the structures. Branching rate was calculated from total number of junctions divided by vessel area, and the end-point rate was calculated from the total number of end points divided by vessel area (Bernklau, Lucas, Jekle, & Becker, 2016; Erturk, Bonilla, & Kokini, 2021; Zudaire et al., 2011).

2.2.10. Ellipsometry

The thickness of the air-water interfacial layer formed by the pulse proteins was measured using an imaging nulling ellipsometer EP4 (Accurion, Germany) (Shen et al., 2023). In short, 15 mL of protein dispersion (0.1 wt%) was added to a Petri dish with a diameter of 6 cm, and the interface was measured for the intensity (amplitude ratio, ψ) and polarization change (phase shift, δ) of an incident polarized laser light beam with wavelength ranging from 499.8 nm to 793.8 nm over two zones at an angle of incidence (AOI) of 50° during the 3 h of interface formation. The output was analyzed by the EP4Model v.3.6.1. software with the Cauchy model, where a refractive index of 1.450 of protein layer was used for interfacial thickness fitting. The measurements were performed in triplicates at room temperature.

2.2.11. Foaming properties

2.2.11.1. Foam overrun. Foam overrun of pulse proteins was measured by whipping 15 mL of protein dispersion (0.1 wt%) at 2000 rpm for 2 min with a frother (Aerolatte, UK). The volume of generated foam divided by 15 mL (and multiplied by 100%) was taken as the foam overrun. Foams were prepared in at least triplicate at room temperature.

2.2.11.2. Foam half-life time. The generated foam by whipping was quickly transferred to a 50 mL gradient cylinder. The cylinder was covered with a film to avoid water evaporation. The time when half of the foam decayed was taken as the foam half-life time. The measurements were performed in at least triplicate at room temperature.

2.2.12. Statistical analysis

One-way analysis of variance (ANOVA) of the data was performed with IBM SPSS Statistics 19. Duncan tests were used for comparison of mean values among determinations using a level of significance of 5%. Standard deviations are calculated for all means, and values are shown as mean value ± standard deviation. Correlation analysis was performed with the same software.

3. Results and discussion

3.1. Physicochemical properties of lentil, faba bean and chickpea proteins

The protein content of faba bean and chickpea protein extracts is 78.9 (± 0.4) wt% and 66.5 (± 0.3) wt%, respectively, slightly lower than that of lentil protein (85.2 ± 0.2 wt%) (Table 1). All protein extracts displayed high protein solubilities at neutral pH, namely 90.2 (± 0.1) % (w/w) for faba bean protein, 83.3 (± 0.3) wt% for chickpea protein, and 91 ± 2 wt% for lentil protein (Table 1). All pulse protein extracts had low phenol (2.0–2.2 wt%), ash (3.0–4.2 wt%) and starch contents (2.4–6.0 wt%) (Table 1), and these compounds are expected to have negligible effects on the interfacial and foaming properties of these pulse proteins. Chickpea protein had a higher oil content (7.0 ± 2.5 wt%) than lentil protein (2.3 ± 0.4 wt%) and faba bean protein (4.1 ± 0.5 wt%) (Table 1), which is ascribed to the higher oil content in chickpea (5 wt%, by producer) compared to lentil (2.2 wt%, by producer) and faba bean (1.13–2.07 wt%) (Choi et al., 2023). The relatively high content of oil in chickpea is expected to exist in the form of oleosomes, which are the natural oil storage organelles of plant seeds (Yang et al., 2021). Such an oil content level was shown to have no apparent influence on the interfacial and foaming properties of other plant protein extracts (Yang et al., 2021) and could be also effectively reduced by membrane filtration (Yang, Berton-Carabin, Nikiforidis, van der Linden, & Sagis, 2022), which was applied later in the protein sample preparation.

The protein composition of these pulse proteins was evaluated by size exclusion chromatography (SEC). According to the SEC chromatograms, all pulse proteins mainly consist of proteins with molecular weights (Mw) of 350–400 kDa and 136–151 kDa (Fig. 1A), which are assigned to 11S legumin globulins and 7S vicilin globulins (Vogelsang-O'Dwyer et al., 2021). Shoulder peaks with Mw of 186–240 kDa are observed between legumin and vicilin peaks (Fig. 1A), and they are assigned to convicilins (Vogelsang-O'Dwyer et al., 2021). A few peaks appear in the low Mw range for all pulse proteins (Fig. 1A), and they are mainly albumins, and the existence of a typical albumin namely lipoxygenase is indicated by the peak with Mw of 70–75 kDa. The peak with Mw around 22 kDa only appears in the chromatogram of chickpea protein (Fig. 1A). This peak also appears in the chromatogram of the chickpea globulin fraction but not in that of the chickpea albumin fraction (Fig. S1). These two protein fractions are separated by acid precipitation. This peak most likely belongs to a disassociated fraction of chickpea globulins. Based on the area of the globulin and albumin peaks, the globulin-to-albumin ratios are 2.5 and 2.2 for faba bean and chickpea proteins, respectively, and equal to 3.8 for lentil protein (Table 2). Since the peaks of the convicilins and vicilins are difficult to separate for faba bean and chickpea proteins, we took the combined area of these two peaks to calculate the legumin-to-(vicilin + convicilin) ratio, and these ratios were equal to 0.7, 1.8, and 0.6 for lentil, faba bean and chickpea proteins, respectively (Table 2).

The nativity of these pulse proteins was evaluated by differential scanning calorimetry (DSC). Faba bean protein showed one denaturation temperature at 90.5 (± 0.1) °C similar to that of lentil protein (87.1 ± 0.4 °C) (Table 2), and these values agree with previous work (94 °C

Table 1
Proximate analysis and protein solubility of lentil, faba bean and chickpea proteins. The averages and standard deviations were the results of at least two replicates.

	Lentil protein	Faba bean protein	Chickpea protein
Protein content (%)	85.2 ± 0.2	78.9 ± 0.4	66.5 ± 0.3
Protein solubility (%)	91 ± 2	90.2 ± 0.1	83.3 ± 0.3
Total starch content (%)	6.04 ± 0.65	4.8 ± 1.1	2.4 ± 0.8
Water content (%)	3.1 ± 0.8	6.3 ± 0.2	2.4 ± 0.3
Ash content (%)	3.03 ± 0.24	3.8 ± 0.3	4.2 ± 0.5
Phenol content (%)	2.00 ± 0.01	2.20 ± 0.11	2.00 ± 0.06
Oil content (%)	2.3 ± 0.4	4.1 ± 0.5	7.0 ± 2.5

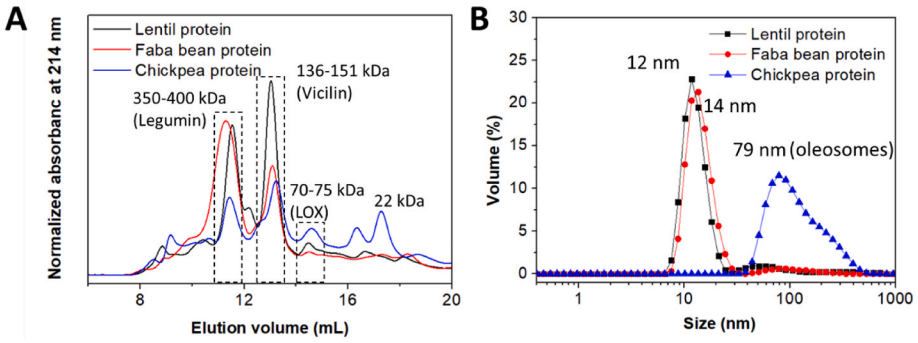

Fig. 1. (A) Size exclusion chromatography (SEC) chromatograms of lentil, faba bean and chickpea proteins in phosphate buffer (20 mM, pH7) containing 150 mM NaCl measured at the wavelength of 214 nm. (B) Particle size distribution of lentil, faba bean and chickpea proteins in phosphate buffer (20 mM, pH7.0) with filtration over 0.22 μm filters. A representative particle size distribution was displayed from three replicates.

Table 2
Molecular properties of lentil, faba bean and chickpea proteins. The globulin-to-albumin ratio, legumin-to-(vicilin + convicilin) ratio, protein fraction contents were calculated based on size exclusion chromatograms. Thermal properties of proteins were measured using differential scanning calorimetry. The averages and standard deviations were the results of at least two replicates.

	Lentil protein	Faba bean protein	Chickpea protein
Globulin/albumin ratio	3.8	2.5	2.2
Legumin/(vicilin + convicilin) ratio	0.7	1.8	0.6
Content of legumin (%)	26.6	40.4	16.9
Content of vicilin + convicilin (%)	39.5	22.7	26.3
Content of albumin (%)	17.6	25.5	25.1
Denaturation temperature at 1_{st} peak (°C)	87.1 ± 0.4	90.5 ± 0.1	81.1 ± 0.4
Denaturation temperature at 2_{nd} peak (°C)	–	–	94.0 ± 0.2
Enthalpy (J/g protein)	8.9 ± 0.4	9.9 ± 0.8	10.1 ± 1.3
Zeta potential (mV)	−18.5 ± 1.2	−13.2 ± 0.8	−12.4 ± 1.2
Relative H_0	1.00 ± 0.00	0.71 ± 0.00	1.11 ± 0.02

and 84 °C for faba bean and lentil protein concentrate, respectively) (Hall & Moraru, 2021). Chickpea protein showed two denaturation temperatures at 81.1 (± 0.4) °C and 94.0 (± 0.2) °C (Table 2), also consistent with previous work (79–82 °C for the first peak, and 90–96 °C for the second peak) (Chang et al., 2022; Yaputri et al., 2023), and the lower temperature was assigned to 7S vicilin globulins, while the higher one was assigned to 11S legumin globulins, since legumins tend to have higher denaturation temperatures than vicilins (Kimura et al., 2008; Withana-Gamage, Wanasundara, Pietrasik, & Shand, 2011). Similar to lentil protein, both faba bean and chickpea proteins have high denaturation enthalpies with values of 9.9 (± 0.8) J/(g protein) and 10.1 (± 1.3) J/(g protein) (Table 2), which are basically consistent with previous work (6–17 J/(g protein)) (Lee, Htoon, Uthayakumaran, & Paterson, 2007; Sharan et al., 2022; Yaputri et al., 2023), where the differences could be caused by the different ratios between legumins and vicilins. These results indicate that faba bean and chickpea proteins are also predominantly in a native state, just like lentil protein.

Particle size, zeta potential and surface hydrophobicity (H_0) of these pulse proteins were also determined. Faba bean and lentil proteins display similar particle size distributions with main peaks at 14 nm and 12 nm, respectively (Fig. 1B), consistent with previous studies (Alavi, Chen, Wang, & Emam-Djomeh, 2021; Jarpa-Parra et al., 2015). The small sizes of faba bean and lentil proteins are ascribed to the major component of globulins in these pulse proteins since the typical diameter of plant globulins is around 10 nm (Fukushima, 1991; Tandang-Silvas et al., 2010). Chickpea protein showed a significantly broader particle size distribution, with a peak at 79 nm (Fig. 1B), which is attributed to the presence of oleosomes, and their larger size most likely dominated the light scattering signal, obscuring the signal from the smaller native chickpea protein. Faba bean and chickpea proteins had a zeta potential at pH 7 of −13.2 (± 0.8) mV and −12.4 (± 1.2) mV, respectively, which was lower than that of lentil protein (−18.5 ± 1.2 mV) (Table 2). Regarding H_0, it increased in the following order: faba bean protein < lentil protein < chickpea protein (Table 2).

3.2. Interfacial adsorption kinetics

The adsorption behavior of lentil, faba bean and chickpea proteins at the air-water interface was measured on both the short timescale (40 ms-4 s) using bubble pressure tensiometer (BPT) (Fig. 2A), and the long timescale (1–10800 s) using automated drop tensiometer (ADT) (Fig. 2B). As shown in Fig. 2A, all three pulse proteins started to increase the surface pressure within the sub-second regime, and the adsorption lag time was 300 ms, 360 ms and 450 ms for lentil, chickpea and faba bean proteins, respectively. This order in the interfacial adsorption rate (lentil protein > chickpea protein > faba bean protein) is highly correlated with the total content of vicilin and convicilin in the extracts (39.5%, 26.3%, and 22.7% respectively), showing a high Pearson correlation coefficient of −0.907. This indicates the 7S vicilin globulin fraction together with the convicilin globulin fraction likely play an important role in the interfacial adsorption of these pulse protein extracts. Lentil, faba bean and chickpea proteins mainly consist of 7S globulins and 11S globulins (Fig. 1 A; Table 2), and 7S globulins have displayed higher surface activities than 11S globulins in several other plant proteins (e.g. pea, soy and Amaranth) (Dagorn-Scaviner, Gueguen, & Lefebvre, 1986; Garcia-Gonzalez, Flores-Vazquez, Barba de la Rosa, Vazquez-Martinez, & Ruiz-Garcia, 2013; Zhu et al., 2020). On the longer timescale (3 h), all three pulse protein extracts increased the surface pressure in similar ways and finally reached a surface pressure of 25.8 (± 0.1) mN/m, 26.3 (± 0.5) mN/m and 27.7 (± 0.3) mN/m, for lentil, faba, and chickpea respectively.

The evolution of the interfacial mechanical properties of all three pulse proteins were also monitored during a period of 5 h, with small amplitude (3%) dilatational rheology. As shown in Fig. 2C, the elastic moduli (E_d') of all samples are already larger than their loss moduli (E_d'') after 3 min of adsorption, indicating the fast development of a solid-like interface for all three pulse proteins. During the first 30 min of adsorption, the E_d' increases substantially in all cases (Fig. 2C), suggesting a fast increase of interfacial stiffness. The curves for lentil and faba flattened off towards a plateau after roughly 3 h of adsorption. The curve for Chickpea showed a minor dip in the value for E_d' after about 30 min, but after 1.5 h started to increase again, to reach a plateau value similar to that of faba. This is most likely an effect of the oscillations on structure formation, where the cyclic expansion and compression of the

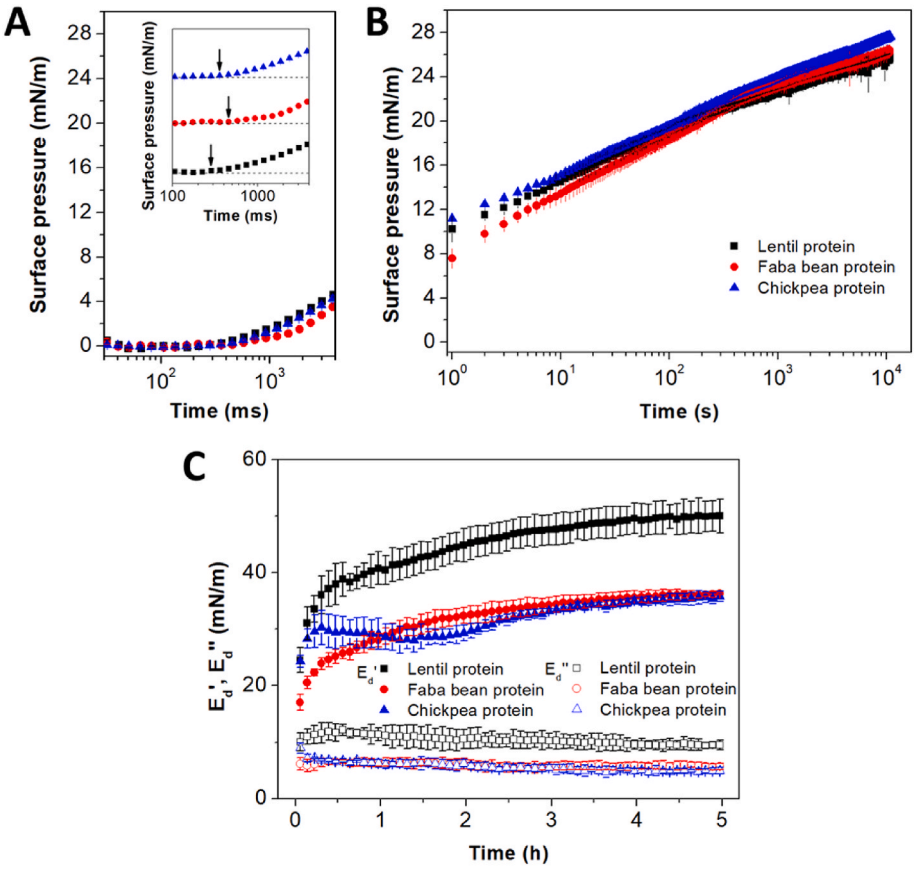

Fig. 2. Surface pressure of lentil, faba bean and chickpea proteins as a function of time within the sub-second regime measured by bubble pressure tensiometer (BPI) (A) and long-time regime measured by automated drop tensiometer (ADT) (B), at the air-water interface at 20 °C. (C) Dilatational elastic modulus ($E_d^{'}$) and viscous modulus ($E_d^{''}$) of the interfaces formed by lentil, faba bean and chickpea proteins with adsorption time measured on ADT at amplitude of 3% and frequency of 0.02 Hz. Protein dispersions containing 0.1 wt% soluble protein were prepared in phosphate buffer (20 mM, pH7) and filtrated through 0.22 μm filters. One representative plot was displayed for each sample from at least three replicates.

interfacial structure during its formation, partially disrupts the structure (Peng et al., 2020). Repeating the experiment at a smaller amplitude would give too much noise, and was therefore not an option. After 5 h of adsorption, $E_d^{'}$ reached values of 50 (± 3) mN/m, 36.3 (± 0.2) mN/m and 35.8 (± 0.9) mN/m for lentil, faba bean and chickpea proteins, respectively, demonstrating that faba bean and chickpea proteins formed interfaces with significantly lower stiffness than lentil protein. The fast formation of solid-like interfacial layers by these pulse proteins was also observed in previous studies (Jarpa-Parra et al., 2015; Meng, Wei, & Xue, 2024; Yang, Liu, Zeng, & Chen, 2018), where the interfaces were formed for 40–60 min and showed stiffness close to this study. The $E_d^{''}$ of all pulse proteins decreased with time within the 5 h of adsorption (Fig. 2C), which suggests a decreasing loss tangent ($\tan\theta = E_d^{''}/E_d^{'}$) and indicates an increase in the elastic contribution of all protein-formed interfaces. This phenomenon has also been observed for chickpea protein by (Meng et al., 2024).

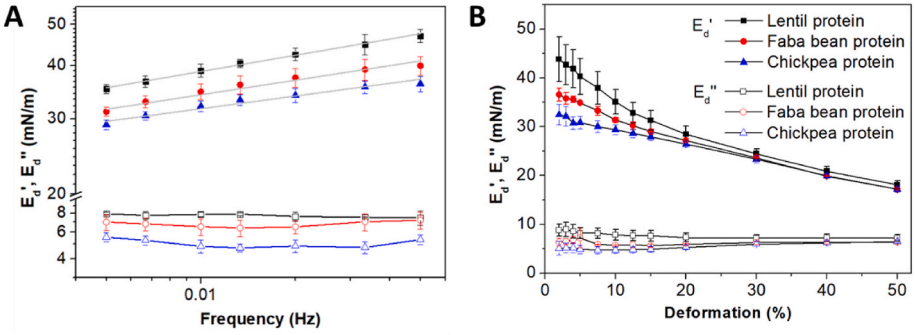

Fig. 3. Dilatational elastic modulus ($E_d^{'}$) and viscous modulus ($E_d^{''}$) of the interfaces formed by lentil, faba bean and chickpea proteins as a function of frequency at a fixed deformation amplitude of 3% (A) or as a function of deformation amplitude at a fixed frequency of 0.02 Hz (B) after 3 h of adsorption of proteins to the air-water interface at 20 °C. The solid lines in Fig. A for $E_d^{'}$ represent power-law fits of the data points ($R^2 = 0.99$ for lentil protein, and 0.98 for both faba bean and chickpea proteins). Protein dispersions containing 0.1 wt% soluble protein were prepared in phosphate buffer (20 mM, pH7) and filtrated through 0.22 μm filters. The averages and standard deviations were the results of at least three replicates.

3.3. Interfacial dilatational rheology

All interfaces after 3 h of adsorption were subjected to interfacial dilatational rheology in both frequency sweeps and amplitude sweeps. In both the frequency sweeps (0.005–0.05 Hz at a fixed amplitude of 3%) and amplitude sweeps (2–50% at a fixed frequency of 0.02 Hz), the $E_d^{'}$ is larger than the $E_d^{''}$ for all three pulses, indicating solid-like behavior of the interfaces. In the frequency sweeps, the $E_d^{'}$ of all pulse proteins follows a power-law behavior with frequency ($E_d^{'} \sim \omega^n$), and the *n*-value is 0.12 (± 0.01), 0.11 (± 0.01) and 0.09 (± 0.01) for lentil, faba bean and chickpea proteins, respectively (Fig. 3A). These n-values are pronouncedly lower than 0.5, the value predicted by the Lucassen-van den Tempel model (Lucassen & Van Den Tempel, 1972), which is valid when the response of the interface to deformation is dominated by the exchange of material between interface and bulk. These low n-values indicate low exchangeability of lentil, faba bean and chickpea proteins at air-water interface, and that these proteins formed disordered solid-like interfacial structures.

In the amplitude sweeps, at 2% amplitude deformation, lentil protein shows the highest $E_d^{'}$, while chickpea protein has the lowest value (Fig. 3B). So, the order of the initial interfacial stiffness is: lentil protein > faba bean protein > chickpea protein. The $E_d^{'}$ at 2% deformation amplitude displays a high Pearson correlation (0.843) with the content of vicilin and convicilin, which suggests vicilin and convicilin might play an important role in forming a stiff interface for these pulse proteins.

Worth mentioning is that, in a previous study, we used a pendant drop method to measure the interfacial properties of lentil protein on a different type of tensiometer, and the $E_d^{'}$ measured at 3% deformation is more than 15 mN/m higher than that measured in this study with a rising bubble method. The large difference on $E_d^{'}$ is mainly ascribed to the drop type. When measuring air-water interfaces, using a pendant drop will have a much larger air volume than using a rising bubble, thus the water evaporation from the interface of a pendant drop will be much more pronounced than that of a rising bubble. The formation of a convex interface from the side of water will also promote water evaporation by increasing the saturated vapor pressure caused by surface tension (Lin, Chen, Zhang, Shen, & Zang, 2019). The water evaporation at the interface can cause an increase of interfacial density by concentration (Al-Milaji & Zhao, 2019), and consequently cause an increase of interfacial stiffness. Such an influence caused by water evaporation can be minimized by decreasing the air space and forming a concave interface via using a rising bubble, as applied in this study. With increasing deformation amplitude, the $E_d^{'}$ of all samples decreases (Fig. 3B), which is attributed to the disruption of the interfacial structures. When the deformation amplitude increases to 30%, the $E_d^{'}$ of all samples start to decrease to similar levels (Fig. 3B), and no longer show a significant difference.

The interfacial elastic modulus ($E_d^{'}$) was derived only from the first harmonic of the Fourier transform of the oscillating surface stress signal, and contributions from high-order harmonics to the behavior of interface were neglected. To unravel more information about the nonlinear behavior of lentil, faba bean and chickpea proteins in interfacial dilatational rheology, Lissajous plots were constructed by plotting surface stress versus intracycle deformation, and these are discussed in the following section.

3.4. Lissajous plots

A dilatational Lissajous plot is a clockwise cyclic plot of stress vs. strain, in which the upper part indicates the extension of the interface, and the lower part indicates the compression of the interface. At 5% amplitude deformation, the Lissajous plots of all three pulse proteins are nearly ellipsoidal and narrow (Fig. 4), suggesting near linear behavior of the interfaces with a dominant elastic component. With increasing deformation amplitude, all Lissajous plots are becoming increasingly wider, indicating an increase of the viscous component, caused by the disruption of interfacial structures (Fig. 4). At 30% amplitude deformation, all Lissajous plots start to show strain softening behavior during extension of the interface (Fig. 4). At 50% amplitude deformation, all Lissajous plots display a high stiffness (i.e. steep slope of the curve) in the beginning of the interfacial extension (Fig. 4) (de Groot et al., 2023). This behavior is followed by a more pronounced strain-softening behavior compared to that in 30% amplitude deformation, as the interfacial structure is disrupted more significantly. These nonlinear

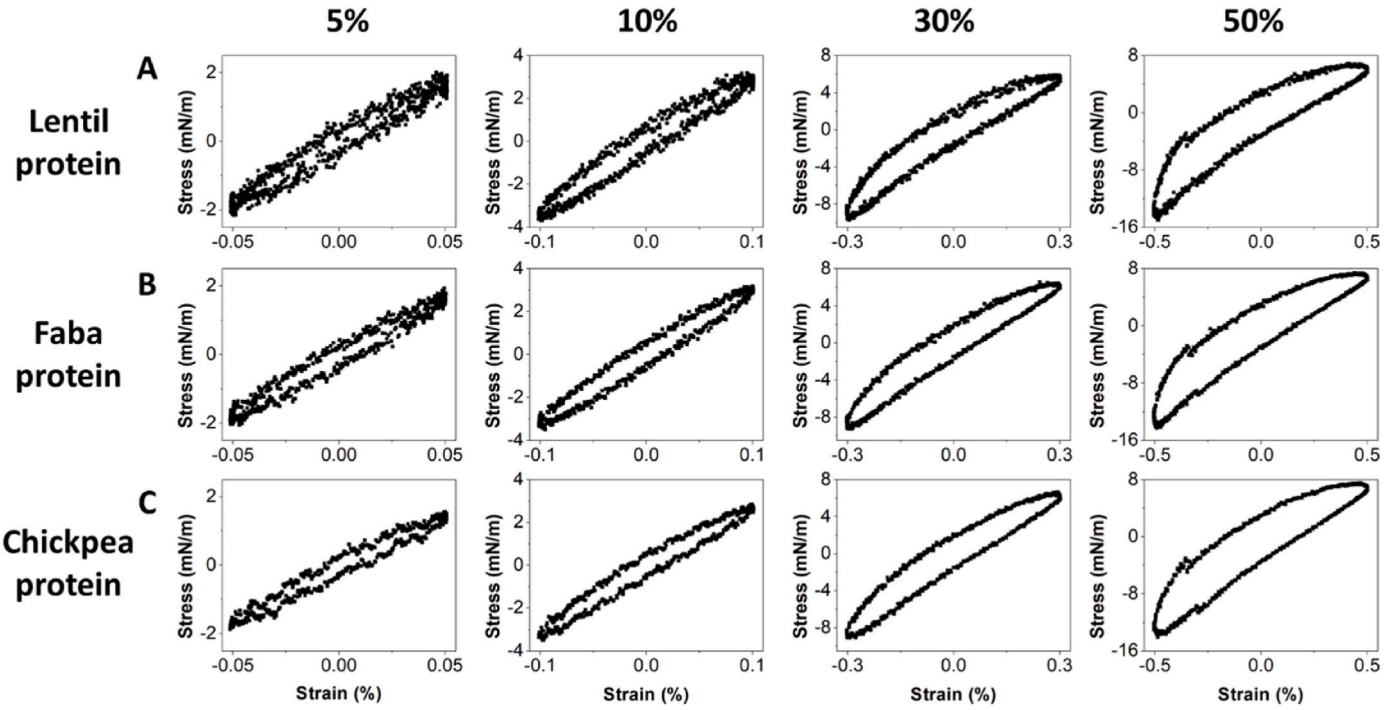

Fig. 4. Lissajous plots of lentil protein (A), faba bean protein (B) and chickpea protein (C) at deformation amplitudes of 5%, 10%, 30% and 50% at a fixed frequency of 0.02 Hz. For clarity, one representative plot or curve was displayed for each condition from at least three replicates.

phenomena seem to be more distinct for the lentil protein-stabilized interface compared to faba bean protein- and chickpea protein-stabilized interfaces (Fig. 4). To further unravel the behavior of these pulse proteins at the air-water interface, quantitative analysis of the Lissajous plots was conducted by using the general stress decomposition (GSD) method as established by de Groot et al. (2023).

3.5. General stress decomposition of Lissajous plots

For the asymmetric plots in Fig. 4, the Fourier transform of the surface stress signal will contain contributions from both odd and even harmonics. The general stress decomposition (GSD) method splits the total surface stress into four components: τ_1, τ_2, τ_3 and τ_4. The stresses $\tau 1$ and τ_2 are the elastic and viscous components of the odd harmonics, and they describe the contributions from interfacial network changes to the overall stress response. The stresses τ_3 and τ_4 are the dissipative (i.e. viscous) and reversible (i.e. elastic) components of the even harmonics, and they describe the contributions due to interfacial density changes to the total surface stress. From these four stress components, several parameters can be established, like the secant moduli of $\tau 1$ ($E_{\tau 1}$) and τ_4 ($E_{\tau 4}$), the vertical shift of τ_4 (γ_s), and the dissipated energies from τ_2 ($U_{\tau 2}$) and τ_3 ($U_{\tau 3}$). These parameters allow us to quantify the relative importance of network disruption and density changes in the nonlinear behavior of the interfaces. For more details on the total stress decomposition principles and procedures, readers are referred to the work published by de Groot et al. (2023).

The Lissajous plots for the decomposed stresses at the 50% deformation amplitude are shown in Fig. 5 as an illustrative examples of the stress decomposition. All $\tau_1+\tau_2$ curves are symmetric with respect to the origin since they only describe the contribution from interfacial network changes. The $\tau_1+\tau_2$ curve of lentil protein has changed from a near ellipsoidal shape at 2% to a rhomboidal shape, whereas this change is less pronounced for faba bean and chickpea proteins (Fig. S2, Fig. 5), suggesting the network structure formed by lentil protein has been disrupted more. All τ_2 curves have similar areas (Fig. 5), resulting in comparable dissipated energies $U_{\tau 2}$ with a value around 6 mJ/m^2 (Fig. 6C). The τ_3 curve of lentil protein shows a slightly larger area than those of faba bean and chickpea proteins (Fig. 5), corresponding to a slightly higher dissipated energy $U_{\tau 3}$ (1.9 ± 0.4) mJ/m^2 than those of faba bean protein (1.5 ± 0.2 mJ/m^2) and chickpea protein (1.2 ± 0.1 mJ/m^2) (Fig. 6D). The τ_4 contribution of lentil protein is more prominent than the others (Fig. 5), corresponding to a more negative elastic modulus of $E_{\tau 4}$ (−8.0 (± 0.7) mN/m compared to those of faba bean protein (−5.0 ± 0.4 mN/m) and chickpea protein (−4.5 ± 0.3 mN/m) (Fig. 6B). At 50% deformation, the absolute value of the stress τ_4 at maximum extension of lentil protein also has a higher proportion in the total stress ($p = 0.002$) with a value of 28.1 (± 0.7) % than both faba bean protein (22.3 ± 1.3%) and chickpea protein (21.0 ± 2.2%). The more pronounced signals from τ_3 and τ_4 for lentil protein-stabilized interfaces indicate that the interfacial density changes play a more distinct role in its surface stress response compared to faba bean protein- and chickpea protein-formed interfaces. The noticeable role of interfacial density changes in interfacial dilatational rheology for lentil protein-stabilized interfaces was also observed in the pendant drop method as used in our previous study (Shen et al., 2024).

We now discuss several quantitative indicators as a function of deformation amplitude derived from the stress decomposition. As shown in Fig. 6, with increasing deformation amplitude, $E_{\tau 1}$ of all pulse proteins decreases (Fig. 6A), which suggests that the interfacial network structure is breaking down, in agreement with the increasing dissipated energy $U_{\tau 2}$ (Fig. 6C). The values of $E_{\tau 4}$ (Fig. 6B) are becoming more negative and $U_{\tau 3}$ (Fig. 6D) increases with increasing amplitude, implying that the contributions due to interfacial density changes are also increasing. Comparing the relative magnitudes of $E_{\tau 1}$ and $E_{\tau 4}$ of all three pulse proteins, we observe that the decrease in $E_{\tau 1}$ is much larger than the decrease in $E_{\tau 4}$ in the whole range of deformation amplitudes, and $U_{\tau 2}$ increases faster and to higher values than $U_{\tau 3}$ with deformation amplitude (Fig. 6A–D), which indicates that the main contributions to the nonlinearities in the surface stress are from interfacial network disruptions. At 2% deformation amplitude, the $E_{\tau 1}$ of lentil protein is higher than that of faba bean and chickpea proteins (Fig. 6A), suggesting that lentil protein forms a stronger network structure at air-water

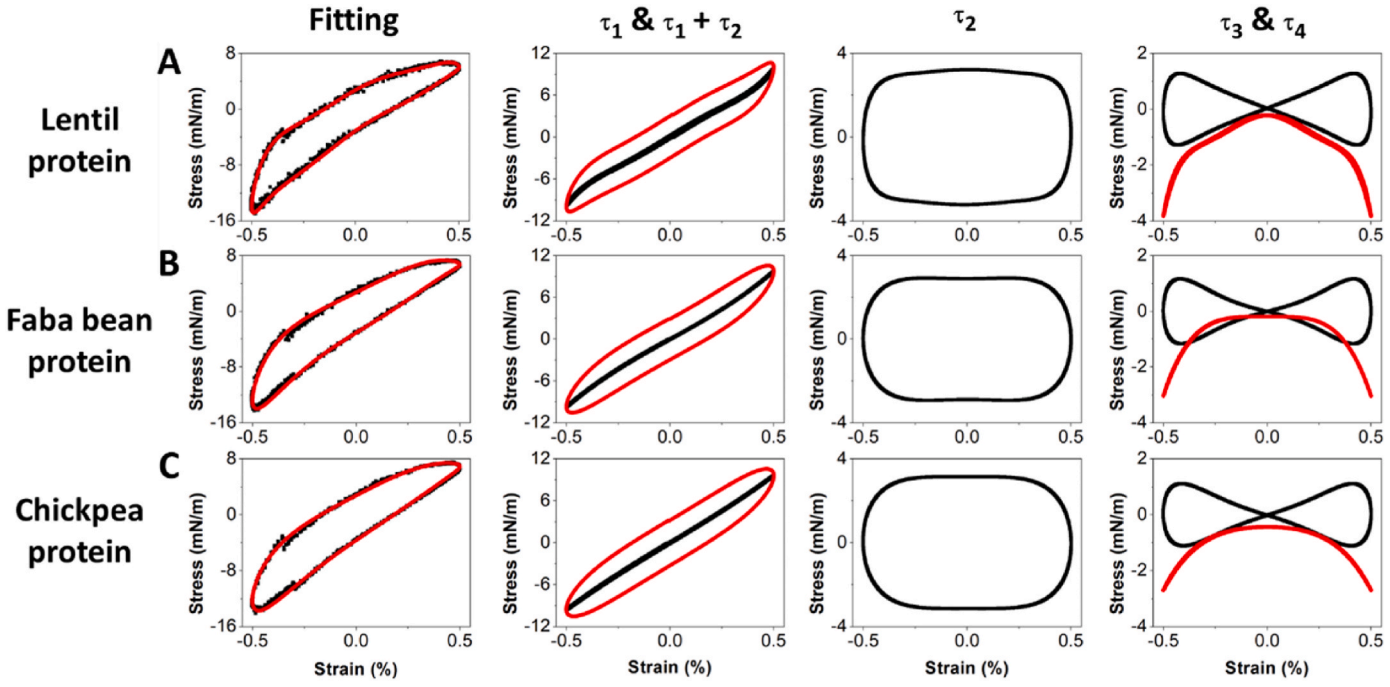

Fig. 5. The Lissajous plots at 50% deformation amplitude were fitted and decomposed into curves of four stress components including τ_1, τ_2, τ_3 and τ_4 versus intracycle deformation for lentil protein (A), faba bean protein (B) and chickpea protein (C). The stresses τ_1 and τ_4 are lines, and the stresses τ_2 and τ_3 are closed loops. For clarity, one representative plot or curve was displayed for each condition from at least three replicates.

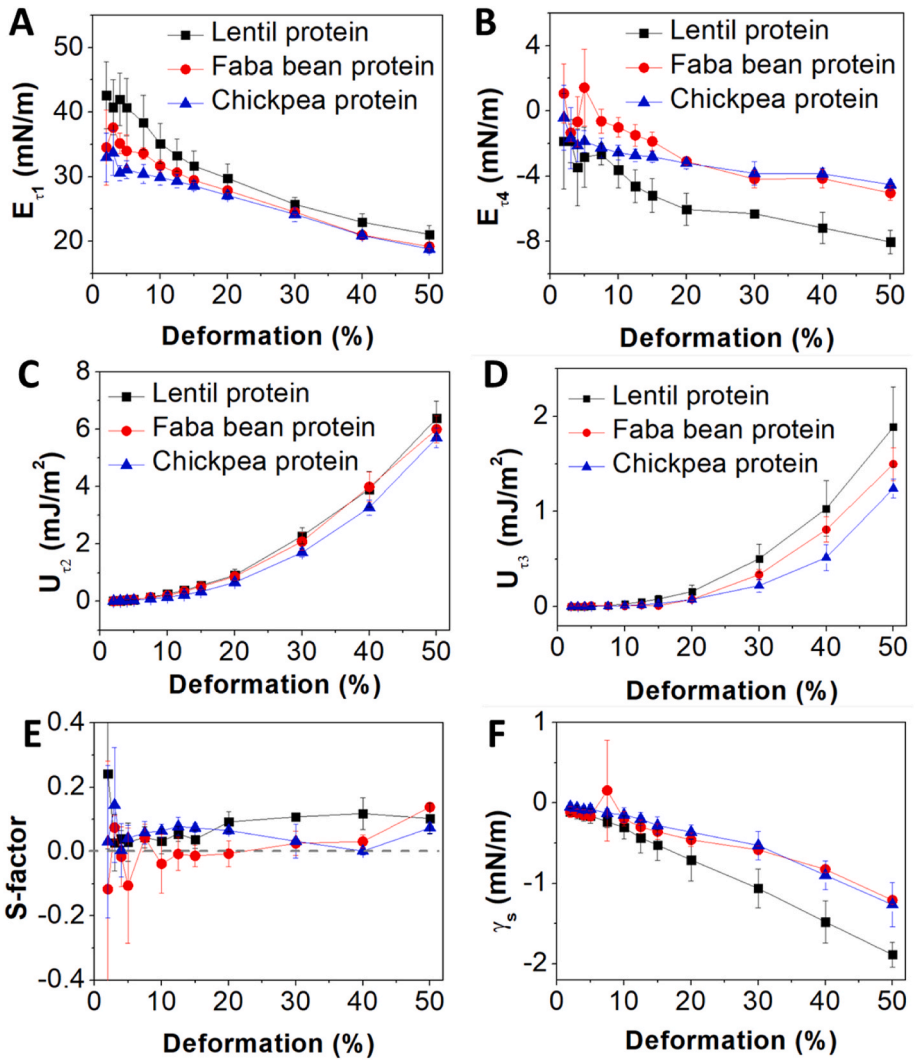

Fig. 6. Modulus of τ_1 ($E_{\tau1}$) (A) and τ_4 ($E_{\tau4}$) (B), and dissipated energy of τ_2 ($U_{\tau1}$) (C) and τ_3 ($U_{\tau3}$) (D), and s-factor (E) and vertical shift (γ_s) of lentil, faba bean and chickpea proteins as a function of deformation amplitude after stress decomposition. The averages and standard deviations were the results of at least three replicates.

interfaces than faba bean and chickpea proteins. With increasing deformation amplitude, lentil protein shows a more negative value increase of $E_{\tau4}$ than both faba bean and chickpea proteins (Fig. 6B). The vertical shift γ_s of all three pulse proteins gently decreases and becomes more negative with increasing strain amplitude (Fig. 6F), suggesting the surface stress oscillates around increasingly lower surface tensions compared to the quasi-equilibrium surface tensions measured after 3 h of adsorption, and the interfaces were slowly driven more and more out of equilibrium by the deformation (de Groot et al., 2023). This phenomenon is more pronounced for lentil protein (Fig. 6F).

Overall, in the interfacial dilatational rheology, interfacial network changes dominate the nonlinearities in the surface stress response for all three pulse proteins. Faba bean protein- and chickpea protein-stabilized interfaces behave rather similar, and the lentil protein-stabilized interface is stiffer and consists of stronger network structure than those formed by faba bean and chickpea proteins.

3.6. Interfacial structures

The interfacial structure of all three pulse proteins was measured by imaging Langmuir-Blodgett (LB) films with atomic force microscopy (AFM) at an area of 2 × 2 μm^2 (512 x 512 pixels^2). The LB films were prepared at two surface pressures, i.e. 13 mN/m and 23 mN/m, equivalent to a dilute (expanded) state and a dense state according to the surface pressure isotherms of these pulse proteins (Fig. S3). In the AFM images, the bright parts represent the distinct structures formed by protein, and the dark regions are voids or flatter structures. Overall, all LB films are heterogeneous (Fig. 7), which agrees with the result from the frequency sweeps in interfacial dilatational rheology (Fig. 3A). All films consist of protein clusters (domains) with a broad size range, and the LB film prepared at 23 mN/m is significantly denser than that prepared at 13 mN/m (Fig. 7). To quantify those interfacial structures, image analysis was performed, including determination of the pair correlation function to determine the characteristic size of protein domains. Network analysis was also performed according to our previous study (Shen et al., 2024). Based on the results of the pair correlation function analysis, all LB films have low level of significant difference (p = 0.085) in the heterogeneous distribution of the protein clusters as indicated by the comparable maximum value of g(r) (Table 3). The LB film of lentil protein at 13 mN/m consists of larger protein clusters (p = 0.003) with a characteristic size of 78 (± 4) nm compared to those of faba bean protein (60 ± 4 nm) and chickpea protein (66 ± 3 nm). While at 23 mN/m, these LB films consist of protein clusters with comparable characteristic size (p = 0.188), and only the LB film of faba bean protein displays an increase of the characteristic size of protein clusters ($p = 7 \times 10^{-12}$) compared to the LB film at 13 mN/m (Table 3).

Regarding the network analysis with Angiotool64, one processed image with identified network structures was exemplified in Fig. S4.

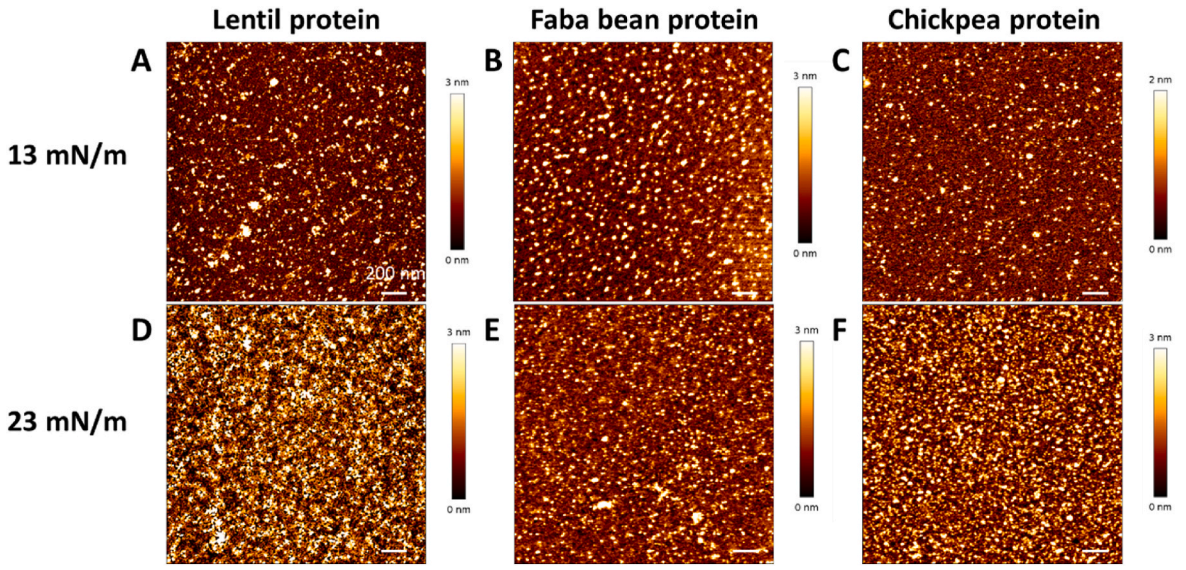

Fig. 7. AFM images of Langmuir-Blodgett films at surface pressures of 13 mN/m (A–C) and 23 mN/m (D–F) for lentil protein (A,D), faba bean protein (B,E) and chickpea protein (C,F) over 2 × 2 μm^2 areas in a lateral resolution of 512 × 512 $pixels^2$. The scale bars indicate a length of 200 nm.

Table 3
Parameters from pair correlation function of the 8-bit grayscale AFM images of lentil, faba bean and chickpea proteins-prepared Langmuir-Blodgett films. Rows with different letters are significantly different ($p < 0.05$).

Langmuir-Blodgett film	Maxima of g(r)	Domain size (nm)
Lentil protein-13 mN/m	1.070 ± 0.002^{a}	78 ± 4^{a}
Faba bean protein-13 mN/m	1.067 ± 0.012^{a}	60 ± 4^{c}
Chickpea protein-13 mN/m	1.046 ± 0.019^{a}	66 ± 3^{bc}
Lentil protein-23 mN/m	1.047 ± 0.005^{a}	76 ± 5^{ab}
Faba bean protein-23 mN/m	1.061 ± 0.026^{a}	70 ± 4^{ab}
Chickpea protein-23 mN/m	1.050 ± 0.013^{a}	68 ± 7^{bc}

According to the network analysis, the LB films of lentil and faba bean proteins have significantly ($p < 0.05$) higher vessel area at 23 mN/m than at 13 mN/m (Table 4), confirming that these LB films are denser at 23 mN/m. The LB films of lentil protein have considerably higher increase of vessel area (11.8%) at 23 mN/m compared to those of faba bean protein (1.8%) and chickpea protein (1.1%), suggesting larger change of interfacial density and agreeing with its pronounced role in the surface stress response of lentil protein (Figs. 5 and 6B). For LB films of lentil proteins, they show a network structure with higher connectivity, longer protein threads, higher level of branching and higher consistency at 23 mN/m than at 13 mN/m, as indicated by the increased junction density, average vessel length and branching rate, and the decreased end-point rate, respectively (Table 4). While the increase of surface pressure overall did not cause significant ($p < 0.05$) difference in the network structure formed by faba bean and chickpea proteins (Table 4).

At the surface pressure of 23 mN/m, the LB film of lentil protein shows higher vessel area (60.6% ± 0.7%) ($p = 5 \times 10^{-5}$) and lower end-point rate (89 ± 13) ($p = 0.002$) than those of faba bean protein (53.1 ± 0.1%; 166 ± 7) and chickpea protein (56.3 ± 0.3%; 122 ± 2) (Table 4), suggesting lentil protein forms denser interfaces with higher consistency. The LB film of lentil protein displays significantly ($p < 0.05$) higher junction density, longer average vessel length and lower lacunarity than those of faba bean protein film (Table 4), implying that lentil protein-stabilized interface has higher connectivity, longer protein threads and a finer structure than the faba bean protein-stabilized interface. While those parameters are comparable with those of chickpea protein film (Table 4), which suggests the interfaces formed by lentil and chickpea proteins have similar connectivity, length of protein threads and heterogeneity in the distribution of network structure. Additionally, the LB films of these three pulse proteins share similar branching rate (Table 4), suggesting these pulse protein-based interfacial network structures have similar level of branching.

To observe the interfacial structure in more details, AFM images were also collected at a smaller area (350 × 350 nm^2) with the same number of pixels. From the AFM images with higher resolution, we observed structures with a size ranging from a few to several tens of

Table 4
Parameters from network analysis of AFM images of lentil, faba bean and chickpea proteins-prepared Langmuir-Blodgett films by AngioTool 64 software. Rows with different letters are significantly different ($p < 0.05$).

Langmuir-Blodgett film	Vessel area (%)	Junction density (junctions/explant area (μm^2))	Average vessel length	Lacunarity	Branching rate	End-point rate
Lentil protein-13 mN/m	48.8 ± 0.9^{e}	226 ± 28^{d}	0.0016 ± 0.0004^{c}	0.0217 ± 0.0014^{a}	464 ± 49^{c}	260 ± 10^{a}
Faba bean protein-13 mN/m	51.3 ± 0.4^{d}	243 ± 6^{cd}	0.0033 ± 0.0009^{bc}	0.0205 ± 0.0009^{a}	475 ± 7^{c}	191 ± 10^{b}
Chickpea protein-13 mN/m	55.2 ± 1.1^{b}	355 ± 13^{ab}	0.0070 ± 0.0032^{abc}	0.0150 ± 0.0005^{c}	644 ± 22^{a}	144 ± 16^{cd}
Lentil protein-23 mN/m	60.6 ± 0.7^{a}	339 ± 32^{a}	0.0141 ± 0.0077^{a}	0.0150 ± 0.0005^{c}	559 ± 53^{b}	89 ± 13^{e}
Faba bean protein-23 mN/m	53.1 ± 0.1^{c}	280 ± 2^{bc}	0.0043 ± 0.0005^{bc}	0.0182 ± 0.0002^{b}	528 ± 6^{bc}	166 ± 7^{bc}
Chickpea protein-23 mN/m	56.3 ± 0.3^{b}	320 ± 5^{a}	0.0121 ± 0.0001^{ab}	0.0156 ± 0.0002^{c}	568 ± 6^{ab}	122 ± 2^{d}

nanometers, connecting to each other and forming a fine-stranded network structure (Fig. 8). The structure units of only a few nanometers mainly appear in the LB films prepared at 13 mN/m (Fig. 8A–C), and the films of chickpea protein prepared at 23 mN/m (Fig. 8D–F), and based on their sizes they are presumably formed by the subunits of legumin and vicilin globulins or the albumin proteins (Fig. 8D–F). The structure units with size of around 10 nm appear only in the LB films prepared at 23 mN/m(Fig. 8D–F), which agrees with the typical diameter of 7S trimer and 11S hexamer plant globulins (Fukushima, 1991; Tandang-Silvas et al., 2010). At the high surface pressure of 23 mN/m, the intact globulin fractions of both lentil and faba bean proteins appear to dominate their interfacial structures (Fig. 8D and E), whereas they are less prevalent in the interfacial structure of chickpea protein (Fig. 8F). Such intact globulin-dominated interfacial structures were also observed on an oat 12S globulin-formed LB film at a high surface pressure of 27 mN/m (Ercili-Cura et al., 2015).

The interfacial thickness of all three pulse proteins were assessed during 3 h of adsorption by using ellipsometry. After 5 min of adsorption, all pulse proteins have already established interfacial layers with thickness of around 4.7 nm, and the value of the thickness mainly shows fluctuations during further adsorption (Fig. S5). This suggests that the interfaces formed by these pulse proteins can enter arrested states quickly, which agrees with the fast development of the solid-like interfaces by these pulse proteins observed in the dilatational time sweeps (Fig. 2C).

Overall, all these pulse proteins are able to generate air-water interfacial layers efficiently and form network structures at the interface. These network structures endow solid-like properties to the interfaces formed by these pulse proteins. Lentil protein is able to form denser air-water interfaces than faba bean and chickpea proteins, which is favorable to a higher interfacial stiffness of lentil protein. The interfacial density changes in lentil protein-stabilized interfaces during expansion and compression give a more significant contribution to the overall surface stress response compared to faba bean and chickpea proteins. Although the interfacial morphology of lentil protein is similar to that of faba bean protein, and its interfacial network structural properties are close to those of chickpea pea proteins, lentil protein clearly has stronger in-plane interactions than both faba bean and chickpea proteins at the air-water interface (Figs. 5 and 6A).

3.7. Foaming properties

Lastly, the foamability and foam stability of faba bean and chickpea proteins were assessed and compared with those of lentil protein. The foamability was indicated by foam overrun after whipping, and the foam stability was compared based on the half-life time of the foam. Chickpea protein displayed a foam overrun with a value of 270%(± 40%), which is comparable with lentil protein (285 ± 17%), while faba bean protein shows the lowest foam overrun with a value of 200% (± 30%) (Fig. 9A). The foam overrun of these pulse proteins was found to have a high Pearson correlation coefficient with their interfacial adsorption lag time (−0.983), which strongly suggests that faster adsorption of pulse proteins to the air-water interface can generate higher amounts of foam. As noted before, a higher vicilin and convicilin content correlates with a faster adsorption rate, and as a result seems to favor a higher foam overrun (Pearson correlation coefficient 0.815). There is also a strong correlation between overrun and Legumin/(vicilin + convicilin) ratio (Pearson coefficient −0.970).

As for foam stability, faba bean and chickpea proteins demonstrate comparable foam half-life time with values of 46 (± 19) min and 38 (± 6) min, respectively, which can be related to the comparable behavior of these two pulse proteins in small and large amplitude oscillatory dilatational rheology at air-water interface (Fig. 2C; Fig. 4B and C; Fig. 5 B, C; Fig. 6). The foam half-life time of these two proteins is much lower than that of lentil protein (115 ± 22 min), indicating much lower foam stability. This could be ascribed to the less stiff and less dense interface formed by faba bean and chickpea proteins compared to lentil protein (Fig. 3B; Table 4). Moreover, we observed high correlation of the foam stability of these pulse proteins with their molecular properties. Vicilins and convicilins seem to play an important role as well in keeping the foam stable, which is indicated by the high Pearson correlation coefficient of foam half-life time with the content of vicilins and convicilins (0.956). Furthermore, the zeta potential of pulse proteins displays a Pearson correlation coefficient of −1.000 and R^2 of −0.999 from linear regression fitting with the foam half-life time, indicating the important role of ζ-potential of pulse proteins in stabilizing foam. Higher ζ-potential will generate higher electrostatic repulsion forces and therewith can better prevent the draining and coalescence of the thin films between adjacent air bubbles (Wang, Nguyen, & Farrokhpay, 2016).

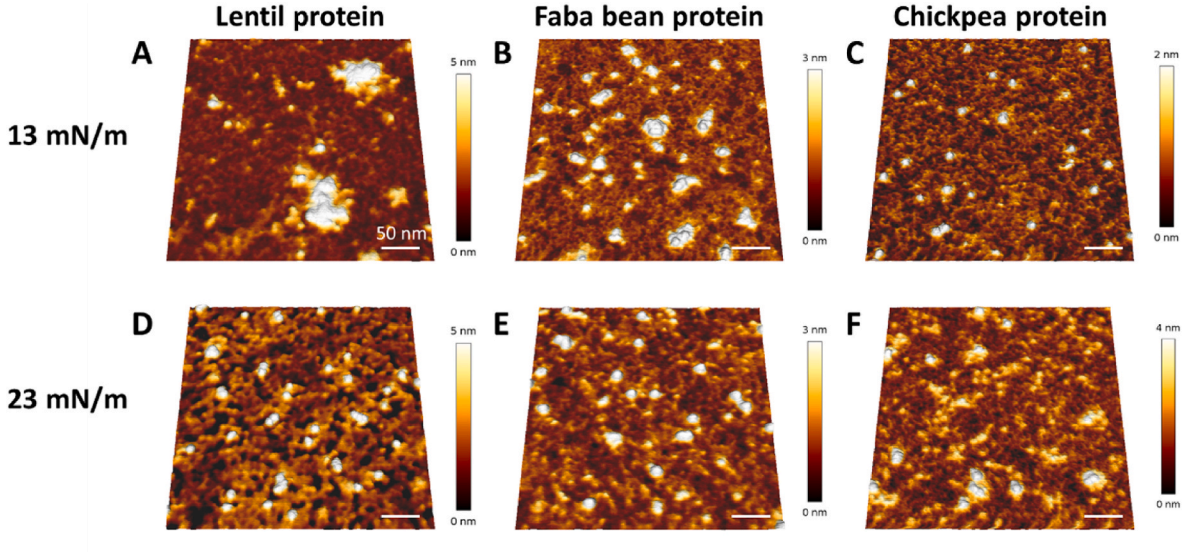

Fig. 8. The 3D AFM images of Langmuir-Blodgett films at surface pressures of 13 mN/m (A–C) and 23 mN/m (D–F) for lentil protein (A,D), faba bean protein (B,E) and chickpea protein (C,F) over 350 × 350 nm^2 areas in a lateral resolution of 512 × 512 $pixels^2$. The scale bars indicate a length of 50 nm.

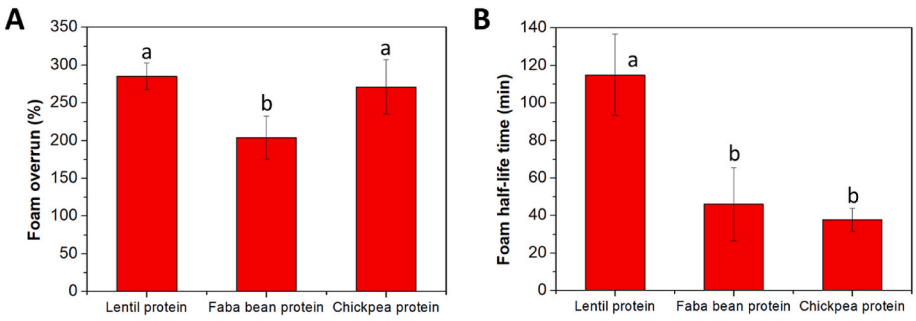

Fig. 9. Foam overrun (A) and foam half-life time (B) of lentil, faba bean and chickpea proteins. Protein dispersion containing 0.1 wt% soluble protein was prepared in phosphate buffer (20 mM, pH7) at 20 °C and filtrated through 0.22 μm filters. The averages and standard deviations were the results of at least three replicates. Columns with different letters are significantly different ($p < 0.05$).

4. Conclusion

This study systematically investigated the similarities and differences of the whole protein extracts from lentil, faba bean and chickpea, from the perspective of their molecular and air-water interfacial properties, and linked them to their foaming properties. These pulse proteins were obtained by simple alkaline extractions and have high protein content, high protein solubility, high nativity and low aggregation levels. They are rich in globulins and albumins, where globulins are the dominant protein components, consisting of 11S legumins and 7S vicilins. These pulse proteins adsorbed to air-water interface in sub-seconds, and their adsorption lag time displayed high negative Pearson correlation coefficient with the foamability and the content of vicilin and convicilin. Lentil protein has the highest vicilin and convicilin content and showed the shortest adsorption lag time of 300 ms, and consequently demonstrated the highest foam overrun of 290%. All pulse proteins form viscoelastic solid-like interfaces at the air-water interface and showed fast formation of an arrested state. These interfaces are disordered and consist of heterogeneous network structures, which are primarily comprised of intact globulins for lentil and faba bean proteins and seemingly mixtures of intact globulins and protein subunits/albumins for chickpea protein. Lentil protein barely appears to unfold at the air-water interface, similar to faba bean protein, while these proteins formed different interfacial network structures with different dilatational rheological behaviors. Chickpea protein seems to partially unfold at the interface while displaying similar interfacial network structural properties as lentil protein. But chickpea protein-stabilized interfaces demonstrated clearly different mechanical properties compared to lentil protein-stabilized interface. It remains an open question how the exact changes in interfacial structure are related to the details of the molecular structure of the protein.

Finally, the ζ-potential, interfacial stiffness and interfacial density of these pulse proteins were found to be highly positively correlated with the foam stability of the pulse proteins, where lentil protein has the best performance, while faba bean and chickpea proteins have comparably lower performance. We show the important role of a comprehensive understanding of the molecular properties and interfacial behavior of plant proteins in understanding their macroscopic foaming properties. Vicilin globulin might be a key component for pulse proteins to exert their foaming performance. In view of the small sample size (n = 3), the correlations should be seen only as an indicator; further testing is required to confirm the relationships among the relevant parameters. These findings are expected to provide clear directions to screen and use pulse proteins for the production of aerated food products with desired properties. To better understand the behavior of these pulse proteins at air-water interface and in foam formation and stabilization, the individual behavior of their protein components (e.g. globulins and albumins) warrant further investigation.

CRediT authorship contribution statement

Penghui Shen: Writing – original draft, Visualization, Validation, Software, Methodology, Investigation, Formal analysis, Data curation, Conceptualization. **Jinfeng Peng:** Writing – review & editing, Resources, Project administration. **Leonard M.C. Sagis:** Writing – review & editing, Supervision, Methodology, Funding acquisition, Conceptualization. **Jasper Landman:** Writing – review & editing, Supervision, Methodology, Conceptualization.

Declaration of competing interest

The authors have declared that no competing interest exists. This manuscript has not been published and is not under consideration for publication in any other journal. All authors approve this manuscript and its submission to Food Hydrocolloids.

Data availability

Data will be made available on request.

Acknowledgements

Authors acknowledge Danone Global Research & Innovation Center for the financial support and Joerg Barner for capturing the AFM images of lentil protein films. P. Shen acknowledges the funding from China Scholarship Council (CSC NO. 202006150032).

Appendix A. Supplementary data

Supplementary data to this article can be found online at https://doi.org/10.1016/j.foodhyd.2024.110313.

References

Adarsh, S., Jacob, J., & Giffy, T. (2019). Role of pulses in cropping systems: A review. *Agricultural Reviews, 40*(3), 185–191.

Aiking, H., & de Boer, J. (2020). The next protein transition. *Trends in Food Science & Technology, 105*, 515–522.

Al-Milaji, K. N., & Zhao, H. (2019). New perspective of mitigating the coffee-ring effect: Interfacial assembly. *Journal of Physical Chemistry C, 123*(19), 12029–12041.

Alavi, F., Chen, L., Wang, Z., & Emam-Djomeh, Z. (2021). Consequences of heating under alkaline pH alone or in the presence of maltodextrin on solubility, emulsifying and foaming properties of faba bean protein. *Food Hydrocolloids, 112*.

Alu'datt, M. H., Rababah, T., Alhamad, M. N., Ereifej, K., Gammoh, S., Kubow, S., et al. (2017). Preparation of mayonnaise from extracted plant protein isolates of chickpea, broad bean and lupin flour: Chemical, physiochemical, nutritional and therapeutic properties. *Journal of Food Science and Technology, 54*(6), 1395–1405.

Amagliani, L., Silva, J. V. C., Saffon, M., & Dombrowski, J. (2021). On the foaming properties of plant proteins: Current status and future opportunities. *Trends in Food Science & Technology, 118*, 261–272.

Bernklau, I., Lucas, L., Jekle, M., & Becker, T. (2016). Protein network analysis — a new approach for quantifying wheat dough microstructure. *Food Research International, 89*, 812–819.

Bessada, S. M. F., Barreira, J. C. M., & Oliveira, M. B. P. P. (2019). Pulses and food security: Dietary protein, digestibility, bioactive and functional properties. *Trends in Food Science & Technology, 93*, 53–68.
Boukid, F. (2021). Chickpea (Cicer arietinum L.) protein as a prospective plant-based ingredient: A review. *International Journal of Food Science and Technology, 56*(11), 5435–5444.
Boukid, F., Zannini, E., Carini, E., & Vittadini, E. (2019). Pulses for bread fortification: A necessity or a choice?. *88*, 416–428.
Boye, J., Zare, F., & Pletch, A. (2010). Pulse proteins: Processing, characterization, functional properties and applications in food and feed. *Food Research International, 43*(2), 414–431.
Buhl, T. F., Christensen, C. H., & Hammershøj, M. (2019). Aquafaba as an egg white substitute in food foams and emulsions: Protein composition and functional behavior. *Food Hydrocolloids, 96*, 354–364.
Chang, L., Lan, Y., Bandillo, N., Ohm, J.-B., Chen, B., & Rao, J. (2022). Plant proteins from green pea and chickpea: Extraction, fractionation, structural characterization and functional properties. *Food Hydrocolloids, 123*.
Choi, Y.-M., Yoon, H., Shin, M.-J., Lee, S., Yi, J., Jeon, Y.-a., et al. (2023). Nutrient levels, bioactive metabolite contents, and antioxidant capacities of faba beans as affected by dehulling. *Foods, 12*.
Dagorn-Scaviner, C., Gueguen, J., & Lefebvre, J. (1986). A comparison of interfacial behaviours of pea (Pisum sativum L.) legumin and vicilin at air/water interface. *Food, 30*(3–4), 337–347.
de Groot, A., Yang, J., & Sagis, L. M. C. (2023). Surface stress decomposition in large amplitude oscillatory interfacial dilatation of complex interfaces. *Journal of Colloid and Interface Science, 638*, 569–581.
Detzel, A., Krüger, M., Busch, M., Blanco-Gutiérrez, I., Varela, C., Manners, R., et al. (2022). Life cycle assessment of animal-based foods and plant-based protein-rich alternatives: An environmental perspective. *Journal of the Science of Food and Agriculture, 102*(12), 5098–5110.
Didinger, C., & Thompson, H. J. (2022). The role of pulses in improving human health: A review. *Legume Science, 4*(4), Article e147.
Ehsani, M., Westphalen, H., Doan, H., Lohi, A., & Abdelrasoul, A. (2024). Advancing faba bean protein purification using membrane technology: Current state and future perspectives. *8*(1), 15.
Ercili-Cura, D., Miyamoto, A., Paananen, A., Yoshii, H., Poutanen, K., & Partanen, R. (2015). Adsorption of oat proteins to air–water interface in relation to their colloidal state. *Food Hydrocolloids, 44*, 183–190.
Erturk, M. Y., Bonilla, J. C., & Kokini, J. (2021). Relationship of non-linear rheological properties and quantitative network analysis parameters as a function of increasingly large amplitude deformations in non-fat, low-fat and high-fat yogurt products. *Food Hydrocolloids, 111*, Article 106194.
Fukushima, D. (1991). Structures of plant storage proteins and their functions. *Food Reviews International, 7*(3), 353–381.
Gandhi, H., Toor, B. S., Kaur, A., & Kaur, J. (2022). Effect of processing treatments on physicochemical, functional and thermal characteristics of lentils (Lens Culinaris). *Journal of Food Measurement and Characterization, 16*(6), 4603–4614.
Garcia-Gonzalez, A., Flores-Vazquez, A. L., Barba de la Rosa, A. P., Vazquez-Martinez, E. A., & Ruiz-Garcia, J. (2013). Amaranth 7S globulin Langmuir films and its interaction with l-α-Dipalmitoilphosphatidilcholine at the air–fluid interface. *The Journal of Physical Chemistry B, 117*(45), 14046–14058.
Grasso, N., Lynch, N. L., Arendt, E. K., & O'Mahony, J. A. (2022). Chickpea protein ingredients: A review of composition, functionality, and applications. *Comprehensive Reviews in Food Science and Food Safety, 21*(1), 435–452.
Guemouri, L., Ogier, J., & Ramsden, J. J. (1998). Optical properties of protein monolayers during assembly. *The Journal of Chemical Physics, 109*(8), 3265–3268.
Hall, A. E., & Moraru, C. I. (2021). Structure and function of pea, lentil and faba bean proteins treated by high pressure processing and heat treatment. *Lwt, 152*.
Henn, K., Zhang, X., Thomsen, M., Rinnan, Å., & Bredie, W. L. P. (2022). The versatility of pulses: Are consumption and consumer perception in different European countries related to the actual climate impact of different pulse types? *Future Foods, 6*, Article 100202.
Jarpa-Parra, M. (2018). Lentil protein: A review of functional properties and food application. An overview of lentil protein functionality. *International Journal of Food Science and Technology, 53*(4), 892–903.
Jarpa-Parra, M., Bamdad, F., Tian, Z., Zeng, H., Temelli, F., & Chen, L. (2015). Impact of pH on molecular structure and surface properties of lentil legumin-like protein and its application as foam stabilizer. *Colloids and Surfaces B: Biointerfaces, 132*, 45–53.
Jarpa-Parra, M., Wong, L., Wismer, W., Temelli, F., Han, J., Huang, W., et al. (2017). Quality characteristics of angel food cake and muffin using lentil protein as egg/milk replacer. *International Journal of Food Science and Technology, 52*(7), 1604–1613.
Khiangte, Z., & Siddique, A. (2021). Pulse crops: Steps towards the sustainability in agriculture. *International Journal of Communication Systems, 9*(1), 487–490.
Kimura, A., Fukuda, T., Zhang, M., Motoyama, S., Maruyama, N., & Utsumi, S. (2008). Comparison of physicochemical properties of 7S and 11S globulins from pea, fava bean, cowpea, and French bean with those of soybean—French bean 7S globulin exhibits excellent properties. *Journal of Agricultural and Food Chemistry, 56*(21), 10273–10279.
Kiosseoglou, V., Paraskevopoulou, A., & Poojary, M. M. (2021). Functional and physicochemical properties of pulse proteins. In *Pulse foods* (pp. 113–146).
Kumar, S., & Pandey, G. (2020). Biofortification of pulses and legumes to enhance nutrition. *Heliyon, 6*(3), Article e03682.
Lee, H. C., Htoon, A. K., Uthayakumaran, S., & Paterson, J. L. (2007). Chemical and functional quality of protein isolated from alkaline extraction of Australian lentil cultivars: Matilda and Digger. *Food Chemistry, 102*(4), 1199–1207.
Lin, K., Chen, R., Zhang, L., Shen, W., & Zang, D. (2019). Enhancing water evaporation by interfacial silica nanoparticles. *Advanced Materials Interfaces, 6*(16), Article 1900369.
Lucassen, J., & Van Den Tempel, M. (1972). Dynamic measurements of dilational properties of a liquid interface. *Chemical Engineering Science, 27*(6), 1283–1291.
Martineau-Cote, D., Achouri, A., Karboune, S., & L'Hocine, L. (2022). Faba bean: An untapped source of quality plant proteins and bioactives. *Nutrients, 14*(8).
Meng, Y., Wei, Z., & Xue, C. (2024). Correlation among molecular structure, air/water interfacial behavior and foam properties of naringin-treated chickpea protein isolates. *Food Hydrocolloids, 147*.
Nasrollahzadeh, M., Nezafat, Z., & Shafiei, N. (2021). Proteins in food industry. In M. Nasrollahzadeh (Ed.), *Biopolymer-based metal nanoparticle chemistry for sustainable applications* (pp. 97–136). Elsevier.
Peng, D., Jin, W., Arts, M., Yang, J., Li, B., & Sagis, L. M. C. (2020). Effect of CMC degree of substitution and gliadin/CMC ratio on surface rheology and foaming behavior of gliadin/CMC nanoparticles. *Food Hydrocolloids, 107*, Article 105955.
Raikos, V., Neacsu, M., Russell, W., & Duthie, G. (2014). Comparative study of the functional properties of lupin, green pea, fava bean, hemp, and buckwheat flours as affected by pH. *Food Science and Nutrition, 2*(6), 802–810.
Sharan, S., Zanghelini, G., Zotzel, J., Bonerz, D., Aschoff, J., Saint-Eve, A., et al. (2021). Fava bean (Vicia faba L.) for food applications: From seed to ingredient processing and its effect on functional properties, antinutritional factors, flavor, and color. *Comprehensive Reviews in Food Science and Food Safety, 20*(1), 401–428.
Sharan, S., Zotzel, J., Stadtmüller, J., Bonerz, D., Aschoff, J., Olsen, K., et al. (2022). Effect of industrial process conditions of fava bean (Vicia faba L.) concentrates on physico-chemical and functional properties. *Innovative Food Science & Emerging Technologies, 81*, Article 103142.
Shen, P., Peng, J., Sagis, L. M. C., & Landman, J. (2024). Air-water interface properties and foam stabilization by mildly extracted lentil protein. *Food Hydrocolloids, 147*, Article 109342.
Shen, P., Yang, J., Nikiforidis, C. V., Mocking-Bode, H. C. M., & Sagis, L. M. C. (2023). Cruciferin versus napin – air-water interface and foam stabilizing properties of rapeseed storage proteins. *Food Hydrocolloids, 136*, Article 108300.
Shevkani, K., Singh, N., Chen, Y., Kaur, A., & Yu, L. (2019). Pulse proteins: Secondary structure, functionality and applications. *Journal of Food Science and Technology, 56*(6), 2787–2798.
Shi, D., & Nickerson, M. T. (2022). Comparative evaluation of the functionality of faba bean protein isolates with major legume proteins in the market. *Cereal Chemistry, 99*(6), 1246–1260.
Snyder, C. S., Bruulsema, T. W., Jensen, T. L., & Fixen, P. E. (2009). Review of greenhouse gas emissions from crop production systems and fertilizer management effects. *Agriculture, Ecosystems & Environment, 133*(3), 247–266.
Sosulski, F. W., & Holt, N. W. (1980). Amino acid composition and nitrogen-to-protein factors for grain legumes. *Canadian Journal of Plant Science, 60*(4), 1327–1331.
Tandang-Silvas, M. R. G., Fukuda, T., Fukuda, C., Prak, K., Cabanos, C., Kimura, A., et al. (2010). Conservation and divergence on plant seed 11S globulins based on crystal structures. *Biochimica et Biophysica Acta (BBA) - Proteins and Proteomics, 1804*(7), 1432–1442.
Tang, Q., Roos, Y. H., & Miao, S. (2023). Plant protein versus dairy proteins: A pH-dependency investigation on their structure and functional properties. *Foods, 12*(2).
Vogelsang-O'Dwyer, M., Sahin, A. W., Arendt, E. K., & Zannini, E. (2022). Enzymatic hydrolysis of pulse proteins as a tool to improve techno-functional properties. *Foods, 11*(9).
Vogelsang-O'Dwyer, M., Petersen, I. L., Joehnke, M. S., Sørensen, J. C., Bez, J., Detzel, A., et al. (2020). Comparison of faba bean protein ingredients produced using dry fractionation and isoelectric precipitation: Techno-functional, nutritional and environmental performance. *Foods, 9*.
Vogelsang-O'Dwyer, M., Zannini, E., & Arendt, E. K. (2021). Production of pulse protein ingredients and their application in plant-based milk alternatives. *Trends in Food Science & Technology, 110*, 364–374.
Wang, J., Nguyen, A. V., & Farrokhpay, S. (2016). Effects of surface rheology and surface potential on foam stability. *Colloids and Surfaces A: Physicochemical and Engineering Aspects, 488*, 70–81.
Wierenga, P. A., & Gruppen, H. (2010). New views on foams from protein solutions. *Current Opinion in Colloid & Interface Science, 15*(5), 365–373.
Withana-Gamage, T. S., Wanasundara, J. P. D., Pietrasik, Z., & Shand, P. J. (2011). Physicochemical, thermal and functional characterisation of protein isolates from kabuli and desi chickpea (Cicer arietinum L.): A comparative study with soy (Glycine max) and pea (Pisum sativum L.). *Journal of the Science of Food and Agriculture, 91*(6), 1022–1031.
Yang, J., Berton-Carabin, C. C., Nikiforidis, C. V., van der Linden, E., & Sagis, L. M. C. (2022). Competition of rapeseed proteins and oleosomes for the air-water interface and its effect on the foaming properties of protein-oleosome mixtures. *Food Hydrocolloids, 122*, Article 107078.
Yang, J., de Wit, A., Diedericks, C. F., Venema, P., van der Linden, E., & Sagis, L. M. C. (2022). Foaming and emulsifying properties of extensively and mildly extracted Bambara groundnut proteins: A comparison of legumin, vicilin and albumin protein. *Food Hydrocolloids, 123*, Article 107190.
Yang, J., Faber, I., Berton-Carabin, C. C., Nikiforidis, C. V., van der Linden, E., & Sagis, L. M. C. (2021). Foams and air-water interfaces stabilised by mildly purified rapeseed proteins after defatting. *Food Hydrocolloids, 112*, Article 106270.
Yang, J., Liu, G., Zeng, H., & Chen, L. (2018). Effects of high pressure homogenization on faba bean protein aggregation in relation to solubility and interfacial properties. *Food Hydrocolloids, 83*, 275–286.

Yaputri, B. P., Bu, F., & Ismail, B. P. (2023). Salt solubilization coupled with membrane filtration-impact on the structure/function of chickpea compared to pea protein. *Foods, 12*(8).

Zhao, M., Yang, Q., Zhang, H., Yuan, C., Li, J., Gao, W., et al. (2022). Foaming properties of the complex of chitooligosaccharides and bovine serum albumin and its application in angel cake. *Food Hydrocolloids, 133*, Article 108024.

Zhu, L., Yin, P., Xie, T., Liu, X., Yang, L., Wang, S., et al. (2020). Interaction between soyasaponin and soy β-conglycinin or glycinin: Air-water interfacial behavior and foaming property of their mixtures. *Colloids and Surfaces B: Biointerfaces, 186*, Article 110707.

Zudaire, E., Gambardella, L., Kurcz, C., & Vermeren, S. (2011). A computational tool for quantitative analysis of vascular networks. *PLoS One, 6*(11), Article e27385.